PHYSICS AND RADIATION BIOLOGY

Thallium-201: An Experimental and a Theoretical Radiobiological Approach to Dosimetry

A. I. Kassis, S. J. Adelstein, C. Haydock, and K. S. R. Sastry

Harvard Medical School, Shields Warren Radiation Laboratory, Boston, Massachusetts, and University of Massachusetts, Amherst, Massachusetts

The kinetics of uptake and retention of Tl-201, Rb-86, and K-42 and -43 have been studied in cultured mammalian cells and related to their radiotoxicities. Among the four radionuclides, the intracellular localization of Tl-201, the only emitter of Auger electrons, was important for the manifestation of its cytocidal effects. The results have been found consistent with the short-range nature of Auger electrons and are substantiated by our theoretical dosimetric calculations. The possible implications of this in vitro system for applications of Tl-201 in nuclear medicine are indicated.

J Nucl Med 24: 1164–1175, 1983

The distribution of tissue-incorporated radionuclides is of importance to the dosimetry of internal emitters. Classical dosimetry assumes homogeneous distribution (*1*,*2*) of radionuclides in organs of interest, while presuming that the ranges of particulate radiations (betas and other electrons) are large (*1*,*2*) relative to typical cell diameters (~10 μm). The macroscopic distribution of dose thus calculated has generally served as a sufficient approximation for the energy deposited within the radiosensitive site(s) of a tissue, for example the cell nucleus. However, with the increasing utilization of intracellular agents, such as thallium-201, it has become necessary to examine the microscopic distribution of energy at the cellular level. The likely importance of this for Tl-201 is emphasized by three considerations. (A) Monovalent Tl-201 ions, behaving biologically like potassium cations (*3*,*4*), may be highly concentrated by the cells. (B) The decay of Tl-201 to levels in Hg-201 by electron capture (EC), and by internal conversion (IC) (*5*), leaves vacancies in the inner atomic shells of the daughter Hg atom. As the Hg atom de-excites by radiative x-ray transitions, and, most predominantly, by nonradiative Auger and Coster-Kronig (CK) processes (*6*), a dense shower of low-energy electrons would follow, with electron ranges of subcellular dimensions. Thus, the decay of Tl-201 within an intracellular locus may result in much higher radiation doses to the cell nucleus than that estimated by classical dosimetry. (C) Recent radiobiological studies have revealed enhanced radiotoxic effects of Auger-electron emitters (*7*–*14*), depending on their intracellular locations.

To date, the only Auger-electron emitters studied following their incorporation into DNA have been iodine-125 (*7*–*10*,*13*) and bromine-77 (*14*). When either of these radionuclides is introduced into the DNA of dividing mammalian cells—in the form of the thymidine analogs [5-^{125}I]iododeoxyuridine (^{125}IUdR) or [5-^{77}Br]bromodeoxyuridine (^{77}BrUdR)—it is as efficient in cell killing as densely ionizing radiations of high linear energy transfer (LET), such as alpha particles (*15*). Moreover, recent experiments with [I-125] iodoantipyrine, a tracer that is ubiquitously distributed in cell water, have shown that this tracer does not need to be convalently bound to DNA to exhibit significant radiotoxicity (*11*,*13*). In contrast, an Auger-electron emitter in an extracellular location contributes minimally to cytocidal effects. For example, both sodium iodide (I-

Received Jan. 31, 1983; revision accepted July 21, 1983.

For reprints contact: Dr. A. I. Kassis, Dept. of Radiology, Harvard Medical School, Shields Warren Radiation Laboratory, 50 Binney St., Boston, MA 02115.

125) and sodium bromide (Br-77), which remain extracellular, and also I-125 affixed to plasma membranes, are nontoxic (*9,14,16*). The limited toxicities of the Auger-electron emitters gallium-67 (*10*) and selenium-75 (*12*), which localize in the cytoplasm of cells, confirm further the relative harmlessness of the EC and IC modes of nuclear decay when they occur outside the radiosensitive cell nucleus.

In this work we have studied the kinetics, in cultured mammalian cells, of uptake and retention of the monovalent cations of 73-hr Tl-201 (*5*), 12.4-hr potassium-42 (*17*), 22.4-hr potassium-43 (*18*), and 18.6-day rubidium-86 (*19*). We find that Tl-201 ions are highly concentrated by the cells, as are the other monovalent alkali cations. Our experimental results clearly show that, among the four radionuclides, Tl-201 is the only one whose intracellular localization is important for the manifestation of its lethal effects. In comparison, the radiotoxicity of its cogeners, emitting energetic beta radiations (*17–19*), does not depend on their intracellular location. These results are fully consistent with the short ranges of the Auger electrons emitted following Tl-201 decay, which result in highly localized on-site doses in the vicinity of the disintegrating atom, in contrast to the longer ranges of the sparsely ionizing beta emissions from the other radionuclides. Theoretical estimates of dose rate are presented in substantiation of these findings. Our conclusions are in general agreement with those of Rao et al. (*20*), who have very recently reported on the radiotoxicity of Tl-201 in mouse testis compared with the beta-emitting Tl-204.

MATERIALS AND EXPERIMENTAL METHODS

Cells. Chinese hamster V79 lung fibroblasts were maintained in exponential growth as previously described (*12,14*). Cell-doubling time was approximately 9 hr, with a plating efficiency of 60–80%.

Radionuclides. Thallium-201* was in the form of thallous chloride, essentially carrier-free (specific activity = 2.13 Ci/mg). The specific activities of the chloride salts of K-42, K-43, and Rb-86 were 1.62, 3.43, and 4.0 mCi/mg, respectively.

Uptake studies. Exponentially growing V79 cells were trypsinized and suspended at 200,000 cells/ml in calcium-free minimum essential medium† (MEM) supplemented with L-glutamine (2m*M*), penicillin (50 units/ml), streptomycin (50 μg/ml), 1% nonessential amino acids, and 15% fetal bovine serum (FBS). The lack of calcium in the medium had no effect on the doubling time or survival of V79 cells. Following a 4-hr incubation at 37°C in an atmosphere of 5% CO_2 in air, the cells were sedimented by centrifugation at 2000 rpm for 10 min and resuspended in 4 ml of calcium-free MEM (800,000 cells) containing various concentrations of each radionuclide. The cells were then reincubated at 4°C or 37°C for 18 hr (unless otherwise noted) on an orbital shaker. Despite continuous agitation of the tubes, the cells sedimented to a volume of 0.2 ml within 30 min.

Due to the diffusible nature of these cations, a recently described method for the rapid separation of cells from radioactive media (*21*) was used. Thallium-201 was measured in an automatic gamma scintillation spectrometer, whereas Rb-86 and K-42 and -43 were counted by an indirect method, measuring Čerenkov radiation after the addition of 10 ml of water‡. Counting efficiencies, as determined by counting known volumes of standard solutions spotted on filter-paper discs, were 70, 50, 64, and 40%, respectively, for Tl-201, Rb-86, K-42, and K-43. The reliability of the Čerenkov assay was verified by gamma spectroscopy.

Retention studies. Cells were incubated at 37°C at a single concentration of each radionuclide (35–45 μCi/ml) and the uptake of the cations measured as described above. The cells were then sedimented by centrifugation, resuspended in prewarmed nonradioactive Ca^{++}-free MEM, and reincubated at 37°C in a water bath. Aliquots were sampled immediately and thereafter at several time intervals, the radioactive cell contents being determined and the percentages of retained activities calculated and plotted against time.

Survival assay. Following the 18-hr incubations in radioactive media, the cells were washed and suspended in MEM containing calcium. Cell survival was assayed next by seeding enough cells into 25-cm^2 Falcon tissue-culture flasks to yield 30–250 colonies at 6 days after exposure to the radionuclide. A cell was considered to have survived by its ability to form a colony consisting of 50 or more cells. Three replicates were plated per radionuclide concentration as well as for the nonradioactive controls. Colonies were fixed in Bouin's fixative, stained with trypan blue, air dried, and scored.

Ouabain studies. Uptake and radiotoxicities of Tl-201, Rb-86, and K-43 were also studied in the presence of the cardiac glycoside ouabain. The cells were incubated with various concentrations of ouabain§ in the absence or presence of a constant concentration of each radionuclide (35–45 μCi/ml). The radioactive contents of the cells and the cell survival were determined as mentioned earlier. Since ouabain exhibited mild chemotoxicity to V79 cells under our experimental conditions, the survival fraction (S/S_0) for each ouabain concentration was calculated by dividing the percent growth in the presence of the ouabain by that in its absence.

Temperature studies. Cells were suspended in varying concentrations of Tl-201 and Rb-86 and kept for 18 hr at 4°C or 37°C. At the end of this period, the intracellular concentrations were determined and the cells were assayed for survival. In the absence of the radionuclide, exposing the cells to 4°C for 18 hr had little effect on the plating efficiency.

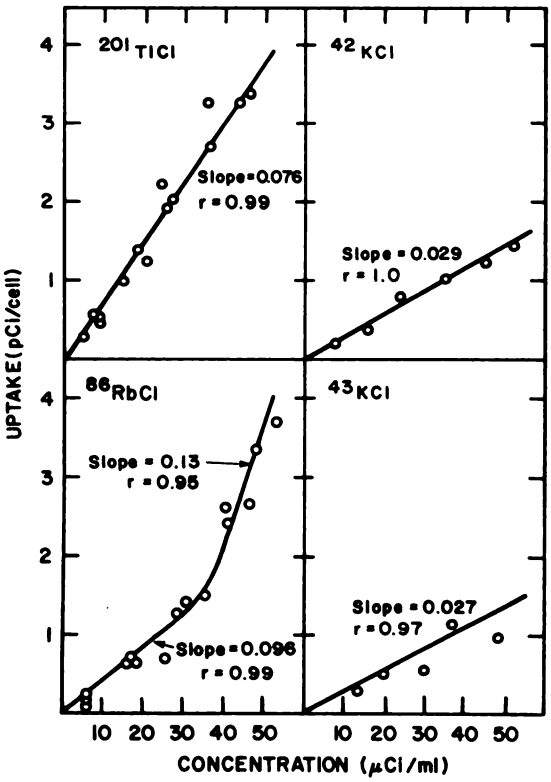

FIG. 1. Uptake (pCi/cell) of Tl-201, Rb-86, K-42, and K-43 by V79 cells as function of concentration of radioactivity (μCi/ml) in extracellular medium. Each point represents average of three replicates.

EXPERIMENTAL RESULTS

Kinetics of uptake and retention of Tl-201, Rb-86, K-43, and K-42. Uptake of the four emitters by V79 cells following an 18-hr incubation is plotted in Fig. 1 as a function of concentration in the external medium. Within the range studied, the cellular uptakes of Tl-201, K-43, and K-42 were linear, with the curves exhibiting correlation coefficients of 0.97 or higher. Rubidium-86 uptake was linear up to a concentration of about 40 μCi/ml followed by a steeper slope at higher concentrations. Both K-43 and K-42 had similar slopes that were much lower than those of Tl-201 and Rb-86. This difference is not surprising since the medium in which the cells are incubated is high in potassium (0.4 mg of KCl/ml).

The extent to which these cations are concentrated by V79 cells is shown in Table 1, following the conversion of intracellular content in pCi/cell to μCi/ml (V79 cells have a volume of 570×10^{-12} cc/cell, see Ref. *12*). Both Tl-201 and Rb-86 were almost 130 times as concentrated inside the cells as in the extracellular environment. Potassium-43 and -42 were concentrated only fiftyfold, presumably due to the effective decrease of their specific activities in the presence of large amounts of stable potassium in the medium.

Figure 2 plots the rates of uptake of the four radionuclides by V79 cells following various incubation periods at 37°C. All four cations showed similar overall uptake profiles, the rate being most rapid within the first half hour. The influx slowed thereafter, and by 6 hr a near-equilibrium between the efflux and influx rates was attained. As expected, a single curve was representative of both K-43 and K-42, whose total uptakes were significantly lower than those of Tl-201 and Rb-86.

The percent radioactivity retained by the cells after separation from radioactive medium is illustrated in Fig. 3. The efflux rates of these cations following 18-hr incubations had two separate components: an immediate efflux that was most pronounced for potassium and least for thallium, and a slower rate of release that was most rapid for thallium.

To determine whether the rapid efflux rate of thallium was due to cellular membrane damage secondary to intracellular irradiation, cells were incubated with Tl-201 for various periods before the measurement of efflux rate. No differences were observed.

Clonal survival. The survival of exponentially growing suspensions of V79 cells was determined by the colony-forming assay. The survival fractions (S/S_0) were plotted as a function of the average radioactivity (pCi/cell) measured in whole cells (Fig. 4). All curves were characterized by an initial shoulder, with Tl-201 (the only Auger emitter) exhibiting the greatest radiotoxicity, as characterized by D_{37} and D_0 (Table 2).

Temperature effects. Figure 5 illustrates the effects of incubation at lower temperature (4°C) on the uptakes and radiotoxicities of Tl-201 and Rb-86. As expected, the decreased metabolic rates at 4°C significantly lowered the uptakes of both cations. When the survival fraction was plotted against the concentration of the radionuclide in the external medium, the radiotoxicity of Tl-201 was reduced, whereas that of Rb-86 was not affected. These experiments demonstrate the strong dependence of the radiotoxicity of the Auger-electron emitter on its intracellular localization.

Ouabain effects. To demonstrate further the importance of the intracellular concentration to radiotoxicity of thallium-201, the active uptake of the radionuclides was specifically inhibited by incubating the cells in the

TABLE 1. INTRACELLULAR TO EXTRACELLULAR CONCENTRATION RATIOS OF K-42, K-43, Rb-86, AND Tl-201 IN V79 CELLS

Radionuclide	$[\mu Ci/ml]_{int}$	$[\mu Ci/ml]_{ext}$	Int/ext
K-43	711	15	47
K-42	762	15	51
Rb-86	1842	15	123
Tl-201	2001	15	133

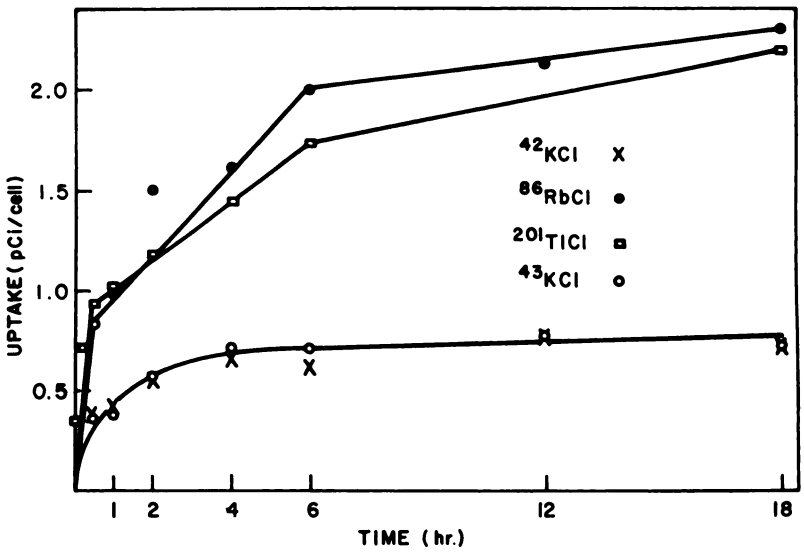

FIG. 2. Uptake (pCi/cell) of Tl-201, Rb-86, K-42, and K-43 by V79 cells as function of duration of incubation at 37°C. Each point represents average of three replicates.

presence of ouabain, a drug that interferes with the energy-dependent sodium-potassium ATP-ase pump. Uptakes of K-43, Rb-86, and Tl-201 were reduced by incubating the cells in various concentrations of the drug (Fig. 6). The uptakes of potassium and thallium fell to <25% of the former level, whereas that of rubidium was decreased to less than half. However, whereas the radiotoxicities of both K-43 and Rb-86 were not significantly altered by the decrease in their intracellular concentrations, the survival fraction of Tl-201-incubated cells was increased 400-fold at higher ouabain concentrations, again illustrating the importance of the intracellular localization of this Auger-electron emitter in regard to its radiotoxic effects.

THEORETICAL ESTIMATES

In this section we estimate theoretically the radiation dose rates to the cells due to nonpenetrating radiations from the decay of each radionuclide. The dosimetric considerations are preceded by a presentation of the necessary data on these radiations.

Beta emission from K-42 and -43, and Rb-86. These beta-decaying radionuclides are well investigated, and the relevant information is summarized in Table 3. The average beta energies ($\bar{E}_\beta$) are calculated assuming the usual statistical (Fermi) distribution (*22*) in most cases, and including, when necessary, additional energy-dependent spectral-shape factors for once-forbidden β^- transitions. The primary information on all radiations, including minor β^- transitions and gamma photons, not listed in Table 3, may be found in Martin and Blichert-Toft (*17*) for K-42, Benczer-Koller et al. (*18*) for K-43, and Tepel (*19*) for Rb-86. The average ranges in Table 3 correspond to radii of spheres of tissue-equivalent material (water), centered around a point source, in which 90% of the average β^- energy is absorbed. These estimates are made using Berger's approach (*23*).

Electron spectrum in Tl-201 decay. *Current status.* Nass (*24*) and Kocher (*25*) have tabulated data on ra-

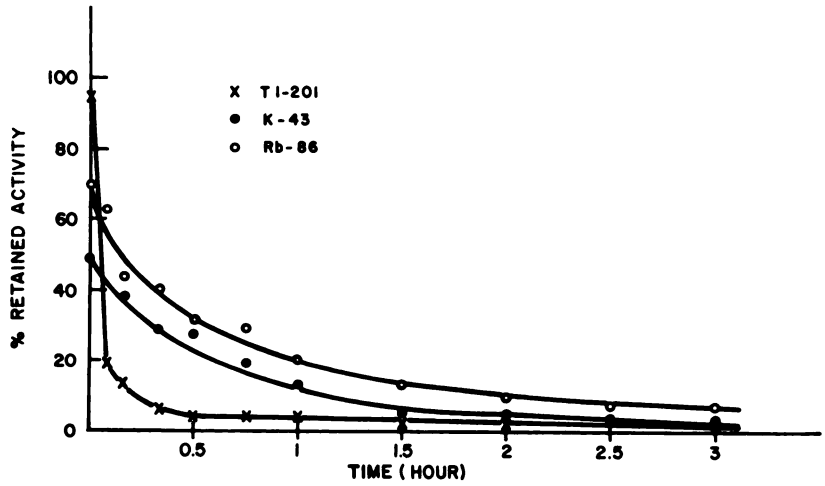

FIG. 3. Retention of Tl-201, Rb-86, K-42, and K-43 by V79 cells following 18-hr incubation with 40 μCi/ml of each radionuclide. Each point represents average of three replicates.

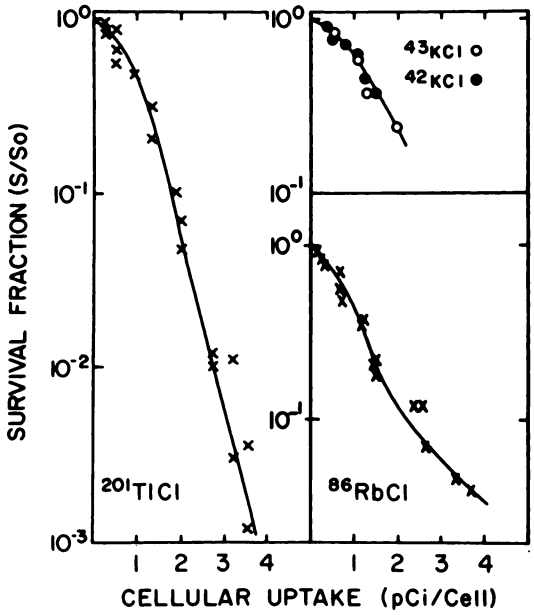

FIG. 4. Survival curves for V79 cells following 18-hr exposure to Tl-201, Rb-86, K-42, and K-43. Survival fractions (S/S_0) are plotted as function of cellular uptake (pCi/cell). Each point represents average of three replicates.

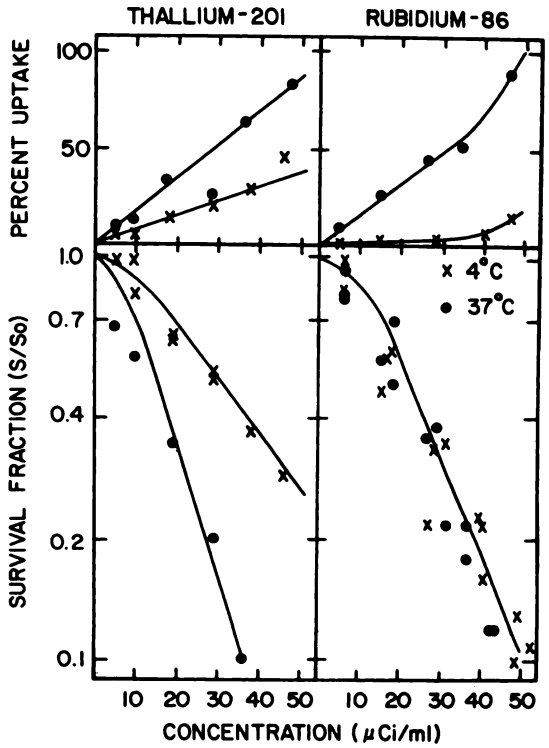

FIG. 5. Uptake and survival curves for V79 cells following 18-hr incubation with Tl-201 or Rb-86 at 37°C or 4°C. Uptake (percent) and survival fractions (S/S_0) are plotted as function of extracellular radioactivity concentration (μCi/ml).

diations from the decay of Tl-201, but their data on Auger electrons are scanty. Recently Rao et al. (*20*) have presented a detailed average theoretical spectrum of Auger and CK electrons to be expected following the decay of Tl-201. In arriving at those estimates, they used the electron-binding energies tabulated by Bearden and Burr (*26*). This classic compilation of core-level binding energies is based mainly on data from x-ray spectroscopy. Since this method gives differences in binding energies, significant calibrational errors may creep into the individual values of the binding energies. Indeed, a recent compilation (*27*) of the binding energies, obtained more directly for 44 metallic elements, reveals important deviations from the Bearden-Burr values (*26*). We have evaluated the Auger- and CK-electron spectra (Table 4) using the new core-level binding energies given by Fuggle and Mårtensson (*27*).

Nuclear and atomic information. The basic information and ideas involved in these calculations are briefly summarized: (a) The branching ratios for EC decay to levels in Hg-201, and the yields of various electromagnetic transitions in Hg-201, are taken from the recent compilation by Schmorak (*5*). (b) The EC probabilities in the various atomic shells are calculated theoretically (*17,22*). Table 5 gives the average distribution of primary inner-shell vacancies in the Hg daughter atom due to EC. (c) The average primary-vacancy distribution from IC, given in Table 5, is calculated using the nuclear decay data (*5*) and the internal conversion coefficients (ICC) of Rösel et al. (*28*). The average yields and energies of conversion electrons, obtained concomitantly, are listed in Table 6.

TABLE 2. RADIOTOXICITIES OF K-42, K-43, Rb-86, AND Tl-201 IN V79 CELLS, IN pCi/CELL. PARENTHESES SHOW CORRESPONDING RADIONUCLIDE CONCENTRATIONS (μCi/ml) IN INCUBATION MEDIUM

Radionuclide	D_{37}	D_0
Tl-201	1.2 (17.5)	0.4 (5)
Rb-86	1.2 (27.5)	2.7 (12)
K-42	1.5 (55)	
K-43	1.5 (64)	

The primary K-shell vacancies (Table 5) are filled predominantly (~97%) by radiative x-ray transitions (*6*). The radiative probabilities for L-shell vacancies are significantly smaller (≤30%) for heavy elements (*6*), and negligible for vacancies in higher shells. The major mechanisms of de-excitation are nonradiative. These transitions are of the Auger and CK type (*6*), or are even super-CK in nature (*29*), involving emission of electrons from the atom. The CK and super-CK transitions, whenever they are energetically possible, overwhelm the Auger mode.

In addition to the primary-vacancy distribution (Table 5) and the new binding energies (*27*), we have used the following atomic data in obtaining the results in Table

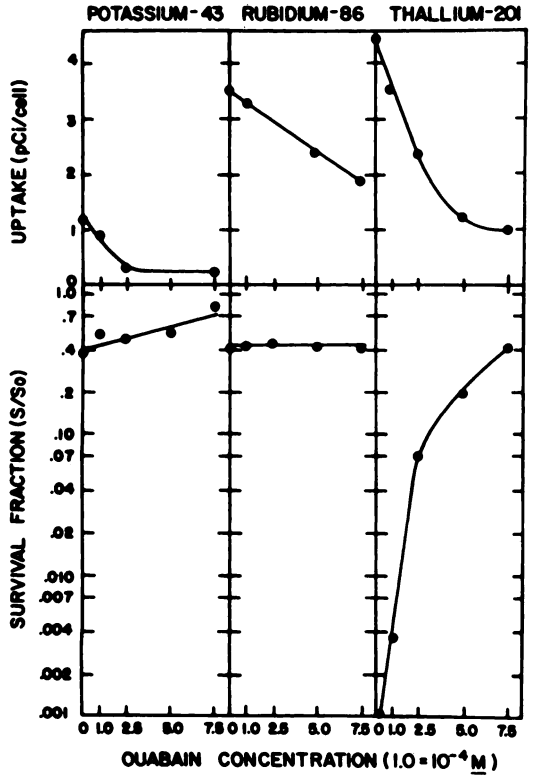

FIG. 6. Uptake and survival curves for V79 cells following 18-hr incubation with Tl-201, Rb-86, and K-43 in presence of various concentrations of ouabain. Uptake (pCi/cell) and survival fractions (S/S_0) are plotted as function of ouabain concentration (M) in extracellular medium. Each point represents average of three replicates.

4. For the K-shell and L-shell transitions, we used the relativistic x-ray emission rates of Scofield (*30*) and the recent relativistic radiationless transition rates of Chen et al. (*31*). The Auger, CK, and super-CK rates given by McGuire in the independent particle picture for the M and N shells (*32,33*) are used for vacancies in these shells. Vacancies in the O shell of Hg can be filled only by super-CK transitions, since in an aqueous solution the P shell of Hg^{2+} is empty. There are no theoretical calculations available yet for the O shell. The O_1 vacancies are assumed to be filled by $O_1O_2O_{4,5}$, $O_1O_3O_{4,5}$, and $O_1O_{4,5}O_{4,5}$ super-CK transitions in proportion to the statistical weights of the O_2, O_3 and $O_{4,5}$ levels. Possible effects of multiple holes on the binding energies are ignored, as they were in McGuire's calculations. Since the Hg atoms are in the condensed phase, we have made the reasonable assumption that no appreciable charge buildup occurs as a result of the atomic cascades. All Auger-electron energies are obtained as differences between the relevant binding energies. The L-shell CK-electron energies are from the tables of Chen et al. (*34*). The CK and super-CK electron energies for the other shells are calculated using the "Z(Z + 1) rule" (*35*).

Remarks on radiations from Tl-201 decay. Several comments are appropriate concerning these radiations.

1. The gamma photon and the K and L x-ray yields that we have estimated (not given here) are the same as in the table of Nass (*24*).

2. The $M_{4,5}$ vacancies have a small probability (*6*) of about 2.5% of being filled radiatively. The average yield of these photons (~2.0 keV) is only 5 per 100 decays of Tl-201.

3. The average conversion-electron spectrum in Table 6 provides more detail than the spectrum reported previously (*24*). Since the theory of IC is well established, and ICC values are now available for all shells (*28*), any future changes in the conversion-electron spectrum should result in the reassessment of the primary data on population of the 1.57-keV first excited state (*5*) in Hg-201. The feeding of this level (11.4%) through cascade transitions (*5*) in Hg-201 is clear. Although it is quite well established that this 1.57-keV level and the Hg-201 ground state are *together* populated directly through EC with a 50% (*5*) probability, we do not know the exact amount of its direct feeding by EC. In view of this, we simply assumed equal branching of EC decay to the two levels of interest in Hg-201. Rao et al. (*20*) and Nass (*24*) also adopted the same position. Kocher (*25*) assumed no feeding of the 1.57-keV level by EC.

4. The Auger- and CK-electron spectrum following Tl-201 decay is very complex indeed. Data in Table 4 are a concise presentation of this spectrum, with electron groups of comparable energies grouped together. The average energies given are the weighted average values. These data agree with the spectrum calculated by Rao et al. (*20*), with only small but significant differences in the average energies of some of the very low energy groups. This is consistent with the differences in the electron-binding energies used in the two calculations.

5. The point raised in paragraph 3 regarding the population at the 1.57-keV level is also relevant to the data in Table 4. However, this transition is converted

TABLE 3. SUMMARY OF MAJOR BETA EMISSIONS IN THE DECAY OF K-42, K-43, AND Rb-86

Radionuclide	Beta energy in keV maximum	Beta energy in keV average	Intensity (%)	Average 90% range (cm) in water
K-42	3520	1566	82.1	0.86
	1995	823	17.6	0.42
K-43	1240	477	3.7	0.24
	820	295	87.0	0.13
	460	150	8.0	0.06
Rb-86	1775	709	91.2	0.38
	700	233	8.8	0.10

TABLE 4. THEORETICAL ESTIMATES OF AVERAGE AUGER- AND CK-ELECTRON SPECTRUM FOLLOWING DECAY OF Tl-201

No.	Transition	Yield per 100 decays	Average energy in keV	Range (μm) in unit-density matter (*37*)
1	$N_{6,7\ A}$, $O_{1\ CK}$, $N_{2\ CK}$	219	0.023	0.0012
2	$O_{1,3\ CK}$, $N_{2\ CK}$, $M_{2\ CK}$, $N_{6,7\ A}$	296	0.042	0.0027
3	$O_{2\ CK}$, $M_{3\ CK}$, $L_{1\ CK}$	46	0.061	0.0038
4	$N_{6,7\ A}$, $O_{1\ CK}$, $N_{1,2,3\ CK}$, $M_{1\ CK}$	689	0.082	0.0047
5	$N_{2,3,4,5\ CK}$, $M_{2,3\ CK}$, $L_{1\ CK}$	280	0.157	0.0075
6	$N_{1,2,4,5\ CK}$, $N_{4,5\ A}$, $M_{1,2\ CK}$	90	0.260	0.0120
7	$N_{2,3,4\ CK}$, $M_{3\ CK}$	50	0.427	0.020
8	$L_{1\ CK}$, $M_{1,2\ CK}$, $N_{1\ A}$	22	0.709	0.038
9	$L_{2\ CK}$, $M_{1\ CK}$	5.6	1.371	0.100
10	M_A, $L_{1\ CK}$	212	1.874	0.170
11	L_A	79	8.47	2.30
12	K_A	3.4	61.07	65.0

only in the N and O shells, and the primary vacancies (Table 5) through this pathway are considerably fewer than deeper-shell primary vacancies. Since the latter are multiplied much more than the former via the atomic cascades, the effect of a significant revision of the population of the 1.57-keV level on the total Auger and CK spectrum should be rather modest. Further, there is reasonable experimental support (*36*) for the main features of the theoretical calculations (*33*) on the important N-shell transitions in elements in the region of Hg. Accordingly, the data of Table 4 constitute a reasonable first approximation of the Auger- and CK-electron spectrum in Tl-201 decay.

Dosimetric considerations. *Qualitative implications.* In Tables 4 and 6 we have included the average ranges of the various electron groups in unit-density matter. These are based on the experimental data of Cole (Table III, Ref. *37*). Out of a total of about 21 electrons released per Tl-201 decay on the average, about 20 have ranges of 2 μm or less, out of which about 16 have ranges of $\pm$0.01 μm. Very few ($\sim$0.3) have ranges of 50 μm or more. This is in contrast to the energetic β^- particles of macroscopic ranges (Table 3) in the case of the other cations. It is also well known that the average LET of these betas is very small compared with LET values of about 10–25 keV/μm for electrons of very low energy (*37*). These considerations indicate the very short range of action of electrons from Tl-201, involving only submicroscopic regions in the immediate vicinity of the decay site. Accordingly, decays of Tl-201 occurring inside the cell should be highly efficient in causing biological effects, whereas extracellular decays are practically nontoxic. Avid intracellular concentration of Tl-201 by tissues, as quantified by the uptake studies, would only lead to high radiotoxicity. On the other hand, the radiotoxicity of K-42 and -43, and Rb-86, should be independent of their cellular concentrations. Experiments at 37°C and 4°C, and those in the absence or presence of ouabain, readily demonstrate the validity of these expectations.

Calculations of dose rate. We present here detailed calculations of average dose rates to V79 cells, and estimates of dose rates to cells in a simulated tissue. The cells are assumed to be spheres of 10.3 μm diameter (*12*), the various cations being uniformly distributed inside the cells. The cells and the medium are treated as unit-density matter.

At any instant, there are three contributions to the total dose rate R (rad/hr) to the cell: from disintegrations occurring inside the cell itself, from disintegrations in other cells, and from those in the extracellular medium. Thus

TABLE 5. AVERAGE INNER-SHELL VACANCY DISTRIBUTIONS IN DAUGHTER Hg ATOM AFTER EC AND IC TRANSITIONS IN Tl-201 DECAY

Mode	Shell									
	K	L_1	L_2	M_1	M_2	N_1	N_2	N_3	O_1	O_2
EC	75.4	17.6	1.3	4.4	0.4	0.7	0.1	—	0.01	—
IC	23.3	17.3	1.7	3.9	0.5	31.9	3.5	0.4	3.1	0.3
Total	98.7	34.9	3.0	8.3	0.9	32.6	3.6	0.4	3.11	0.3

TABLE 6. AVERAGE INTERNAL-CONVERSION ELECTRON SPECTRUM IN Tl-201 DECAY

No.	Energy of transition (keV)	Conversion-electron group	Yield per 100 decays	Average energy (keV)	Range (μm) in unit-density matter (*37*)
1	1.57	N	33.4	0.786	0.045
		O	3.4	1.454	0.11
2	27.0	L	0.15	12.24	4.2
		MNO	0.05	24.02	14.0
3	30.6	L	8.2	15.84	6.5
		MNO	2.5	27.74	18.0
4	32.19	L	7.0	17.43	7.5
		MNO	2.2	29.34	20
5	135.34	K	7.5	52.24	50
		LMNO	1.7	123.40	220
6	165.88 }	K	15.8	84.30	110
	167.43 }	LMNO	3.4	155.3	325

$$R = A\Delta(r_c\phi_{c\to c} + r_o\phi_{c\to o} + r_m\phi_{c\to m}). \quad (1)$$

In Eq. (1), A is the radioactivity in μCi/g, averaged over the cells and the medium, Δ is the mean energy per decay in g·rad/μCi·hr, ϕ is the particular absorbed fraction, and r the relative concentration of activity compared with the average value. The subscripts c, o, and m refer, respectively, to the target cell, other cells, and the extracellular medium. Let the cells occupy a fraction f of the total volume, and let them concentrate radioactivity by a factor C relative to the value in the extracellular medium. We then have

$$r_m = 1/[Cf + (1 - f)], \text{ and } r_c = r_o = Cr_m. \quad (2)$$

For Tl-201, with discrete electron energies, $\Delta = 2.13 \times 10^{-3}\Sigma n_i E_i$ (*2*), where E_i (keV) is the average energy of the ith group, with yield n_i per decay (Tables 4 and 6), and has the value of 0.0925 g·rad/μCi·hr. For the beta emitters, Δ is calculated taking account of the beta-particle continuum (*12*). For K-42, K-43, and Rb-86 the corresponding values of Δ are 3.05, 0.66, and 1.42 in g·rad/μCi·hr.

The absorbed fraction $\phi_{1\to 2}$ is the fraction of the energy emitted in Region 1 that is absorbed in Region 2. In writing Eq. (1) for the dose rate to the cell, the use of the quantities $\phi_{c\to o}$ and $\phi_{c\to m}$, which specify that the cell is the source region, is justified by the reciprocal dose theorem (*38*), and has the advantage that ratios of source-to-target volume do not appear in the expressions. The absorbed fractions are calculated using the relation

$$\phi_{1\to 2} = (1/E)\int_0^\infty \psi(r)(d\epsilon/dr)dr, \quad (3)$$

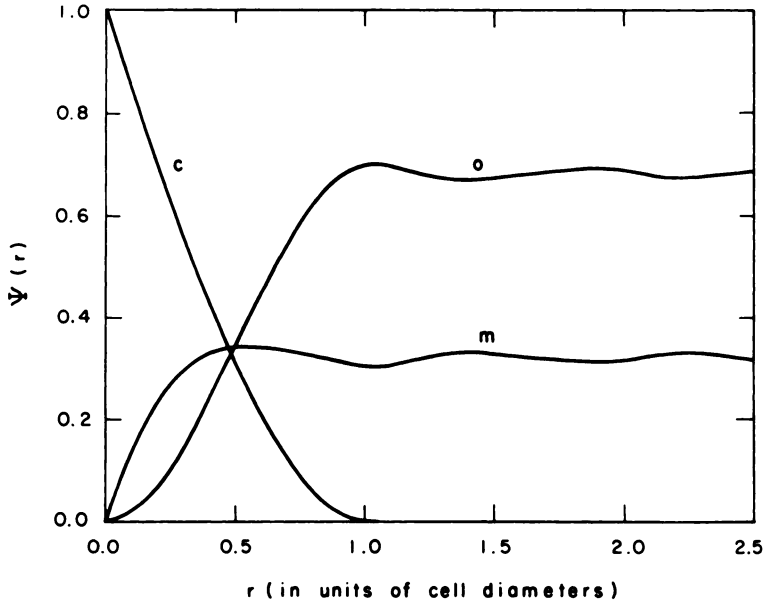

FIG. 7. Geometric factor $\psi(r)$ plotted against radial distance r, in units of cell diameter, for simulated tissue geometry. Note that pair distance distribution function (*38*) is given by $4\pi r^2\psi(r)/V_t$. Quantity V_t is volume of target region, consisting of body-centered cubic array of target cells external to single spherical source cell. Curves designated by c, o, and m represent $\psi_{c\to c}(r)$, $\psi_{c\to o}(r)$, and $\psi_{c\to m}(r)$, respectively. For simulated tissue geometry, sum of these three functions is unity for any value of r.

where E is the average energy of nonpenetrating radiations in the decay of each species, obtained from Tables 4 and 6 for Tl-201 and from Table 3 for the others. The geometric factor $\psi(r)$ is the mean probability that a randomly directed vector, of length r, that begins at a random point in Region 1 will end within Region 2. As an example, these geometric factors, calculated for a body-centered cubic array of target spheres, are shown in Fig. 7. The point isotropic differential absorption $d\epsilon/dr$ is multiplied by dr to obtain the average energy absorbed in the annular region of the spherical shell with radii r and r + dr, when a point source of the radionuclide is located at the origin. The point isotropic specific absorbed fraction is given by $(d\epsilon/dr)/4\pi r^2\rho E$, the density ρ being taken as unity. It is adequate for our present purpose to calculate $d\epsilon/dr$ using Cole's data (*37*), with the simplifying assumption that the emitted particles travel radially outward from the site of decay.

Of the two geometries considered in these calculations, the tube geometry (TG) is relevant to the present in vitro studies, and the simulated tissue geometry (STG), is of possible interest for a highly cellular organ. In the former case, 800,000 cells, each of volume 570 μm^3, are assumed to be uniformly distributed throughout a ~0.2-ml volume of cell-culture medium in a polypropylene tube. The cells thus occupy only a small fraction, $f = 2.28 \times 10^{-3}$, of the total volume. In STG, spherical cells are considered to be packed in an infinite body-centered cubic array, where each cell touches its eight nearest neighbors. In this geometry, f = 0.680.

In the calculation of $\phi_{c\to c}$ for spherical cells, the geometric factor in Eq. (3) is given by (*39*)

$$\psi(r) = 1 - (3r/2d) + (1/2)(r/d)^3$$

where $0 \le r \le d$ (the cell diameter)

$$\psi(r) = 0 \text{ when } r > d \qquad (4)$$

This function, shown in Fig. 7 by Curve c, is the same for cells in either of the two geometries. Accordingly, $\phi_{c\to c}$ calculated for each given radionuclide is the same in both geometries.

In obtaining $\phi_{c\to o}$ and $\phi_{c\to m}$, it is useful to consider the sum

$$\phi_{c\to c} + \phi_{c\to o} + \phi_{c\to m} = \phi_{c\to t} \qquad (5)$$

Physically, $\phi_{c\to t}$ is the average fraction of the energy emitted within a cell and absorbed in the total volume containing the cell itself, the other cells, and the extracellular medium. For STG, $\phi_{c\to t} = 1$ since the array of cells is assumed to be infinite. Possible escape of radiation energy has to be considered for the finite case of the tube geometry. The appropriate geometric factor then is that one for which the source volume and the target volume are the same as the total volume. These total self-absorbed fractions, $\phi_{c\to t}$, thus calculated using Eq. (3), are 1.0, 0.78, 0.91, and 0.57 for Tl-201, Rb-86, K-43, and K-42, respectively, in TG.

With $\phi_{c\to t}$ and $\phi_{c\to c}$ obtained as above, the sum $(\phi_{c\to o} + \phi_{c\to m})$ is given by Eq. (5). To obtain individual values of $\phi_{c\to o}$ and $\phi_{c\to m}$, an additional constraint is necessary. In the case of the beta emitters, this relation is evident on inspection of the geometric factors (Curves m and o) in Fig. 7 for STG. For these long-range beta particles of low LET, the ratio of the geometric factor $\psi_{c\to o}(r)$ to $\psi_{c\to m}(r)$ approaches $f/(1-f)$ for distances that are large relative to the cell diameter. Since these low-LET particles deposit very little energy through the first 10 μm around the decay site, it is quite adequate to conclude that $\phi_{c\to o}/\phi_{c\to m} = f/(1-f)$. The same relation should also be valid for the β^- emitters in the case of TG. For Tl-201 in the case of STG, $\phi_{c\to o}$ is calculated using Eq.

TABLE 7. SUMMARY OF THEORETICAL DOSE RATES TO CELLS PER 10 μCi/ml AVERAGE CONCENTRATION OF RADIONUCLIDE

Radionuclide	Absorbed fractions $\phi_{c\to c}$	$\phi_{c\to o}$	$\phi_{c\to m}$	Theoretical dose rates (rad/hr)* Present calculations: $Cell_1$ to $cell_1$	$Cell_0$ to $cell_1$	Medium to $cell_1$	Total to $cell_1$	Classical
Tl-201	0.311	7.9 E-5	0.689	28.9	0.007	0.49	29.4	0.925
		(0.442)	(0.247)	(0.421)	(0.599)	(0.003)	(1.02)	(0.925)
Rb-86	1.42 E-3	8.9 E-5	0.779	2.03	0.13	8.55	10.7	11.1
		(0.679)	(0.319)	(0.03)	(14.1)	(0.05)	(14.2)	(14.2)
K-43	4.07 E-3	1.0 E-4	0.906	1.21	0.03	5.38	6.6	6.00
		(0.677)	(0.319)	(0.04)	(6.51)	(0.06)	(6.6)	(6.6)
K-42	5.16 E-4	6.5 E-5	0.569	0.71	0.09	15.6	16.4	17.4
		(0.680)	(0.320)	(0.02)	(30.2)	(0.3)	(30.5)	(30.5)

* First line of each entry is for tube geometry used in these experiments; second line, with numbers in parentheses, is for simulated tissue geometry.

(3) and $\psi_{c\to o}(r)$ (Fig. 7, Curve o); the ratio $\phi_{c\to o}/\phi_{c\to m}$ then turns out to be 1.8. For Tl-201 in TG, we assume $\phi_{c\to o}/\phi_{c\to m} = f/(1 - f)$, a value perhaps slightly too large but not important enough to introduce significant error in the total dose rate, since f is very small.

Theoretical dose rates. The dose rates to the cells from each of the radionuclide species, calculated as described above, are summarized in Table 7 for an average concentration of radioactivity A = 10 μCi/ml. The results in parentheses are for STG. The contributions from the different sources are indicated explicitly. For Tl-201 and Rb-86, the concentration factor C is taken to be 130, and for K-42 and -43 we have used C = 50, consistent with the experimental results (Table 1). According to classical dosimetry (*1,2*), the dose rates are given by $A\Delta\phi_{c\to t}$. These are included in the last column of Table 7 for A = 10 μCi/ml.

Discussion of theoretical results. The theoretical dose rates to the cells (Table 7) of immediate relevance to the present in vitro studies are those calculated for the tube geometry. The classical macroscopic approach (*1,2*) predicts a very low dose rate for Tl-201. In comparison, the beta emitters are expected to irradiate the cells at about 6 to 20 times the Tl-201 dose rate for any given average concentration of the radionuclides. Our calculations, taking account of the intracellular concentration of these radionuclides, predict cell dose rates that are very different from the "classical" estimates for Tl-201, but only modestly different for the β^- emitters. These results show that Tl-201 has the highest dose rate to the cells, stemming mostly from intracellular contributions due to the low-energy Auger and CK electrons, and accentuated by avid concentration of Tl-201 by the cells. In the case of the β^- emitters, the intracellular component of the dose rate is a relatively minor fraction of the total dose rate in spite of the concentration of these radionuclides by the cells. This is due to the very low LET of the energetic β^- particles. The predominant contribution to the dose rate from these radionuclides comes from decays occurring outside the cell.

Classical dose estimates predict Tl-201 to be almost nontoxic relative to the three β^- emitters, whereas our calculations suggest a high radiotoxicity for Tl-201 when cells are sparsely distributed. The latter expectation is thoroughly borne out by our experiments.

When the fraction of the total volume occupied by the cells is essentially zero, as in these studies, our results show that the cellular dose rate from Tl-201, compared with classical estimates, is enhanced by a factor $N \sim 30$. This is in accord with the dosimetric implications of Tl-201 discussed recently by Rao et al. (*20*). The structure of the theoretical expressions in "Theoretical dose rates" above, shows that the dose-rate enhancement relative to the classical rate depends strongly on f for Tl-201. As f increases, cross irradiations from neighboring cells increasingly contribute to the cellular dose rate, and the assumption of uniform distribution of the radionuclides and radiation energy in the volume—inherent in the classical approach (*1,2*)—tends to become more reasonable. The dose-rate enhancement factor N tends to unity as $f \to 1$. It is not surprising, therefore, that our calculated dose rate to the cells is only about 10% in excess of the classical estimate for the simulated tissue geometry with f = 0.68. For intermediate values of f = 0.01, 0.1, 0.2, and 0.4, we calculate that N = 18.3, 3.6, 2.1, and 1.4, respectively.

What are the implications of this work to realistic situations involving the applications of Tl-201? The answer depends on the role played by f in the organ of interest, given the plausible assumption that Tl-201 may also be as highly concentrated by cells in vivo as in vitro. The only experiment in vivo to date is the work of Rao et al. (*20*), in which Tl-201 or Tl-204 were directly injected into the testes of mice. The biological effects were studied using spermatogenesis as the model. In comparison with the beta dose from Tl-204, they found that the low-energy electrons from Tl-201 were about three times as efficient in causing biological effects, when these effects were compared on the basis of classically predicted doses (*1,2*). They suggest that the higher efficacy of Tl-201 is understandable in terms of a threefold dose-rate enhancement to the cells predicted for $C \sim 100$ and $f \cong 0.1$ to 0.15 (*20*). Our estimates given at the end of the previous paragraph are consistent with such an interpretation. These considerations underline the likely importance of f in Tl-201 cellular dosimetry, and emphasize the need for more radiotoxicity studies of Tl-201 in different in vivo model systems to clarify further the role of f.

Finally, we stress the biological implications of Auger-electron-emitting radionuclides decaying in the vicinity of nuclear DNA in cells (*7–11,13,14*). Using the data of Tables 4 and 6, and the electron ranges and rates of energy loss in unit-density matter (Table III, Ref. *37*), we estimate that about 1.3 keV of energy would be locally deposited in a 5-nm sphere around the decay site of Tl-201, and about 1.7 keV in a 10-nm sphere. Goodhead et al. (*40*) point out that the subcellular radiosensitive loci are of the order of this size, and that localized energy deposition of ~300 eV or more in such regions is necessary for efficient induction of biological effects. The high radiotoxicities of the decay of I-125 and Br-77 in the DNA are consistent with similar values of highly localized energy deposition (*14*). It is therefore plausible that the radiobiological effects of Tl-201 may have been caused by localized dose effects from decays occurring in the proximity of nuclear DNA. Until our understanding of the intracellular distribution of thallium is improved, it is premature to favor this mechanism of localized dose effects over an overall dose enhancement to the entire cell as the likely cause of the strong radiotoxic effects of Tl-201.

SUMMARY AND CONCLUSIONS

From these experiments it is clear that the monovalent cations of potassium, rubidium, and thallium are concentrated by cultured fibroblasts. First, the uptake occurs over a matter of hours ($t_{1/2} \sim 1$ hr) for all the cations. Second, the washouts appear to be biphasic: an immediate washout that is greatest for K (50%), less for Rb (30%), and least for Tl (2.5%); and a second washout that is rapid for Tl ($t_{1/2} \sim 0.1$ hr) and less so for K and Rb ($t_{1/2} \sim 0.5$ hr). Third, the 18-hr uptake of radioactivity is proportional to the concentration in the external medium over a sizeable range (0 to 50 μCi/ml). Fourth, the radionuclides are highly concentrated by the cells relative to the external medium (~fiftyfold for K; ~130-fold for Rb and Tl). These phenomena have permitted us to vary the external and internal concentrations over a range sufficient to produce survival curves to at least 30% in the case of K-42, K-43, and Rb-86, and of 3 log decades in the case of Tl-201. Moreover, the use of ouabain allowed us to drop the internal concentration of K-43 by a factor of 6, of Rb-86 by a factor of 2, and of Tl-201 by a factor of 4, while maintaining a constant external concentration of the radioactive cation of interest.

The relative toxicity of these radioactive species when the cells are separated by large distances compared with their diameters differs significantly from that predicted from standard macroscopic (*1*,*2*) dosimetry considerations. This stems in large measure from the failure of these considerations to take into account the highly localized deposition of energy (*41*) by the Auger and CK electrons resulting from EC and IC during thallium-201 decay. When the radionuclide is concentrated in cells, these electrons are deposited in radiosensitive targets. The macroscopic approach either neglects these low-energy electrons completely or spreads them out over the entire system. In our model, where the cells are spread far apart, an assumption that the energy from these electrons is spread uniformly will grossly underestimate the intracellular dose relative to the extracellular one. In this system, radiation damage is produced primarily by extracellular K-42, K-43, and Rb-86, but conversely, by intracellular Tl-201. As a consequence, macroscopic calculations approximate the toxicity of the potassium and rubidium isotopes while underestimating that of thallium-201.

The situation in intact tissue is, of course, somewhat different, since there some 70% of the volume is cellular. Under these circumstances nearly all the radioactivity is likely to be intracellular, in contrast to our model in which only about 1% is intracellular despite the high intra- over extracellular concentration ratios. Nonetheless, an assumption that the radioactivity is spread uniformly throughout the tissue and that the electrons emitted are absorbed homogeneously would lead to some underestimation of the biologically significant dose, perhaps by a factor of two, depending upon the value of f, as already discussed.

These studies point out the increasing need to take into account the microscopic distribution of dose, on the cellular, nuclear, and even subnuclear scale, as radionuclides distributed in cells become more commonplace—and especially if the decay involves EC or IC. Most of the traditional radiotracers are deposited extracellularly, obviating the necessity for these concerns. As radiotracers are developed for the measurement of intracellular functions and as specific radionuclide therapy is developed, these microscopic considerations should be given greater prominence.

FOOTNOTES

* Kindly provided by New England Nuclear.
† GIBCO, N.Y.
‡ Beckman LS 8000.
§ Sigma.

ACKNOWLEDGMENT

This work has been supported in part by the USPHS Grant CA15523-05 (SJA), and a Biomedical Research Support Grant to the University of Massachusetts, Amherst.

REFERENCES

1. LOEVINGER R, BERMAN M: *A Revised Schema for Calculating the Absorbed Dose from Biologically Distributed Radionuclides. Medical Internal Radiation Dose Committee Pamphlet No 1, revised.* New York, Society of Nuclear Medicine, 1976
2. ICRU Report 32: Methods of assessment of absorbed dose in clinical use of radionuclides. International Commission on Radiation Units and Measurements, Washington, D.C., 1979
3. GEHRING PJ, HAMMOND PB: The interrelationship between thallium and potassium in animals. *J Pharmacol Exp Ther* 155:187-201, 1967
4. GYÖRGY RL, MILNER OT: On some potassium-like qualities of the thallium ion. *Experientia* 24:809-810, 1968
5. SCHMORAK MR: Nuclear Data Sheets for A = 201. *Nucl Data Sheets* 25:193-234, 1978
6. BAMBYNEK B, CRASEMANN B, FINK RW, et al: X-ray flourescence yields, Auger, and Coster-Kronig transition probabilities. *Rev Mod Phys* 44:716-813, 1972
7. HOFER KG, HUGHES WL: Radiotoxicity of intracellular tritium, ^{125}iodine and ^{131}iodine. *Radiat Res* 47:94-109, 1971
8. PRINCE EW, ADELSTEIN SJ: Radiotoxicity of intracellular ^{125}I in mammalian cells: Effect on the survival curve. *J Nucl Med* 13:789, 1972
9. BRADLEY EW, CHAN PC, ADELSTEIN SJ: The radiotoxicity of iodine-125 in mammalian cells. I. Effects on the survival curve of radioiodine incorporated into DNA. *Radiat Res* 64:555-563, 1975
10. HOFER KG, HARRIS CR, SMITH JM: Radiotoxicity of intracellular ^{67}Ga, ^{125}I and ^{3}H. Nuclear versus cytoplasmic radiation effects in murine L1210 leukaemia. *Int J Radiat Biol* 28:225-241, 1975
11. COMMERFORD SL, BOND VP, CRONKITE EP, et al:

Radiotoxicity of intracellular ^{125}I atoms not bound to DNA. *Int J Radiat Biol* 37:547-554, 1980

12. KASSIS AI, ADELSTEIN SJ, HAYDOCK C, et al: Radiotoxicity of ^{75}Se and ^{35}S: Theory and application to a cellular model. *Radiat Res* 84:407-425, 1980
13. BLOOMER WD, MCLAUGHLIN WH, WEICHSELBAUM RR, et al: The role of subcellular localization in assessing the cytotoxicity of iodine-125 labeled iododeoxyuridine, iodotamoxifen, and iodoantipyrene. *J Radioanal Chem* 65:209-221, 1981
14. KASSIS AI, ADELSTEIN SJ, HAYDOCK C, et al: Lethality of Auger electrons from the decay of bromine-77 in the DNA of mammalian cells. *Radiat Res* 90:362-373, 1982
15. BARENDSON GW: Mechanism of action of differnt ionizing radiations on the proliferative capacity of mammalian cells. In *Theoretical and Experimental Biophysics* A. Cole, ed. vol. 1, New York, Dekker, 167-231, 1967
16. WARTERS RL, HOFER KG, HARRIS CR, et al: Radionuclide toxicity in cultured mammalian cells: Elucidation of primary site of radiation damage. *Curr Top Radiat Res Q* 12:389-407, 1978
17. MARTIN MJ, BLICHERT-TOFT PH: Radioactive atoms, Auger-electron, α-, β-, γ-, and X-ray data. *Nucl Data Tables* A8:1-198, 1970
18. BENCZER-KOLLER N, SCHWARZCHILD A, WU CS: Decay of ^{43}K. *Phys Rev* 115:108-114, 1959
19. TEPEL JW: Nuclear data sheets for A = 86. *Nucl Data Sheets* 25:553-602, 1978
20. RAO DV, GOVELITZ GF, SASTRY KSR: Radiotoxicity of thallium-201 in mouse testes: Inadequacy of conventional dosimetry. *J Nucl Med* 24:145-153, 1983
21. KASSIS AI, ADELSTEIN SJ: A rapid and reproducible method for the separation of cells from radioactive media. *J Nucl Med* 21:88-90, 1980
22. BEHRENS A, JÄNECKE J: *Numerical Tables for Beta-Decay and Electron Capture.* Berlin, Springer-Verlag, 1969
23. BERGER MJ: Distribution of absorbed dose around point sources of electrons and beta-particles in water and other media. MIRD Pamphlet No. 7, *J Nucl Med:* Suppl No 5, 5-23, 1971
24. NASS HW: New Tl-201 nuclear decay data. *J Nucl Med* 18:1047-1048, 1977
25. KOCHER DC: *Radioactive decay data tables.* Technical Information Center, U.S. Department of Energy, 181-182, 1981
26. BEARDEN JA, BURR AF: Reevaluation of x-ray atomic energy levels. *Rev Mod Phys* 39:125-142, 1967
27. FUGGLE JC, MÅRTENSSON N: Core-level binding energies in metals. *J Electron Spectrosc Relat Phenom* 21:275-281, 1980
28. RÖSEL F, FRIES HM, ALDER K, et al: Internal conversion coefficients for all atomic shells, ICC values for Z = 68-104. *Atomic Data and Nucl Data Tables* 21:291-514, 1978
29. MCGUIRE EJ: Auger and Coster-Kronig transitions. In *Atomic Inner-Shell Processes.* Crasemann B, ed. New York, Academic Press, vol. 1, pp 293-330, 1975
30. SCOFIELD JH: Relativistic Hartree-Slater values for K and L x-ray emission rates. *Atomic Data Nucl Data Tables* 14: 121-127, 1974
31. CHEN MH, CRASEMANN B, MARK H: Relativistic radiationless transition probabilities for atomic K- and L-shells. *Atomic Data Nucl Data Tables* 24:13-37, 1979
32. MCGUIRE EJ: M-shell Auger, Coster-Kronig, and radiative matrix elements, and Auger and Coster-Kronig transition rates in j-j coupling. *Research Report:* SC-RR-710835, Sandia Laboratories, 1972
33. MCGUIRE EJ: N-shell Auger, Coster-Kronig, and radiative matrix elements, and Auger and Coster-Kronig transition rates in j-j coupling. *Report SAND*-75-0443, Sandia Laboratories, 1975
34. CHEN MH, CRASEMANN B, HUANG K-N, et al: Theoretical L-shell Coster-Kronig energies, $11 \leq Z \leq 103$. *Atomic and Nucl Data Tables* 19:97-151, 1977
35. CHUNG MF, JENKINS LH: Auger electron energies of the outer shell electrons. *Surf Sci* 22:479-485, 1970
36. MATTHEW JAD, NETZER FB, BERTEL E: The $N_{4,5}N_{6,7}N_{6,7}$ and $N_{4,5}N_{6,7}O_{4,5}$ Auger spectra of Au, Pt and Ir. *J Electron Spectrosc Relat Phenom* 20:1-10, 1980
37. COLE A: Absorption of 20-eV to 50,000-eV electron beams in air and plastic. *Radiat Res* 38:7-33, 1969
38. LOEVINGER R, JAPHA EM, BROWNELL GL: Discrete radioisotope sources. *In Radiation Dosimetry*, Hine GJ, Brownell GL, eds. New York, Academic Press, pp 693-799, 1956
39. BERGER MJ: Beta-ray dosimetry calculations with the use of point kernels. *In Medical Radionuclides: Radiation Dose and Effects.* Cloutier RJ, Lowell Edwards C, Snyder WS, eds. USAEC Report CONF-691212, 63-86, 1970
40. GOODHEAD DT, THACKER J, COX R: Effectiveness of 0.3 keV ultrasoft carbon X-rays for the inactivation and mutation of cultured mammalian cells. *Int J Radiat Biol* 36:101-114, 1979
41. WRENN ME, PARRY HOWELLS GP, HAIRR LM, et al: Auger electron dosimetry. *Health Phys* 24:645-653, 1973